Investigation of Structural and Magnetic Properties of Multiferroic $La_{1-x}y_xfeo_3$perovskites, Prepared by Citrate Auto-Combustion Technique

Yehia M. Abbas, Ahmed B. Mansour, Shehab E. Ali, Ahmed H. Ibrahim*

Physics Department, Faculty of Science, Suez Canal University, Ismailia, Egypt

Abstract

In this work, we studied the structural and magnetic properties of multiferroic $La_{1-x}Y_xFeO_3$ perovskites, (x= 0.0, 0.05, 0.1, 0.15, 0.25 and 0.3) which synthesized through Sol-gel auto-combustion technique using a citric acid as a fuel. The room temperature synchrotron X-ray diffraction (XRD) analysis revealed that the all the synthesized samples consisted of the polycrystalline orthorhombic structure perovskites (space group pnma), and tolerance factor confirmed the phase stability of the prepared perovskite system. The Williamson-Hall plot based on synchrotron XRD data were employed to estimate the average particle diameter and varies from 18 nm to 27.8 nm. For a deeper insight of the crystal structure, high resolution transmission microscopy imaging (HRTEM) was performed. The estimated values of crystallite size from HRTEM and synchrotron XRD data were coincident. Many of crystallographic parameters and electron density measurements were calculated by Rietveld refinement of synchrotron XRD data. $La_{1-x}Y_xFeO_3$ perovskite crystals are canted antiferromagnets with a weak ferromagnetism in room temperature. The magnetic properties were gotten through analyzing the magnetization versus temperature M(T) and M(H) hysteresis loop which characterized by a vibrating sample magnetometer (VSM). The molecular structure showed the decrease of the tilting of the octahedra <FeO_6> with increasing Y content trying to strengthen the ferromagnetic character. Selected Area Electron Diffraction (SAED) patterns of the investigated samples exhibited spotty ring patterns, confirming the polycrystalline character. The orthoferrite $La_{1-x}Y_xFeO_3$ crystals are a promising candidate for optical device applications in broad temperature range and high power system.

Keywords

Multiferroic materials, Perovskite, Synchrotron XRD, SAED, Electron density map, Reitveld, FFT.

SUBJECT CLASSIFICATION

Applied crystallography

1. Introduction

The multiferroic materials (MF) showing ferroelectricity (FE) and ferromagnetism (FM) simultaneously have produced an unlimited deal of technological interest during the last decay, due to potential applications in spintronics and information storage and sensors[1-3].The abundance of many MF materials, specially Rare-earth perovskites is related to the production of a magnetic moment due to the existence of the transition metal d electrons, decrease the polar lattice distortion which is essential for ferroelectric behavior[4-6].

Perovskites are mixed oxides with a well-known general formula ABO_3. One of the typical characteristics of this inorganic compounds family is the huge variability of accepted ionic substitutions in crystallography. The tetrahedral sites, so-called (A sites) can be employed by more than 23 elements, while around 50 dissimilar elements are able to inhabit the octahedral (B sites). All these modifications in structure give growth to numerous of the interesting dielectric and magnetic properties of perovskites. In specific, when (B sites) are occupied by Fe^{3+}cations these types of mixed oxides are called orthoferrites.

Lanthanum orthoferrite ($LaFeO_3$) has an antiferromagnetic structure with high Néel temperature (T_N~740 °C)which can be distorted by the substitution of La^{3+} by other trivalent cations, such as Y^{3+}, Gd^{3+}, Sm^{3+} or Yb^{3+}. These rare-earth elements considerably contribute to the complete magnetic response of the orthoferrites. On

the other hand, the substitution with non-magnetic Y^{3+}enables the analysis of the effect of the tetrahedral cation size on the magnetic properties of the perovskites. Overall, the orthorhombic structured $LaFeO_3$ (LFO) shows G-type weak antiferromagnetic ordering below 735 K and transition to ferroelectricity at 475 K [7].

It is a well-known that the whole properties of these materials are analytically dependent on the preparation method. Also the conventional ceramic method, sol-gel auto-combustion method, ball milling and several techniques based on innovative wet-chemistry have been presented [8-10].In these wet chemical methods, pure phase formation can be faster and also the particle size and morphology can be much more controlled. Mechano synthesized $LaFeO_3$ showed a moderately high saturation magnetization, which is associated with the accumulation of several defects in the crystal structure through the mechanical treatment. The replacement of a part of La by Y^{3+} cations increases the structural distortion gradually and creates a significant rise in the magnetization [11].

In our present work, we propose the substitution of lanthanum orthoferrite with yttrium to synthesize $La_{1-x}Y_xFeO_3$ perovskites, (X=0.0, 0.05, 0.1, 0.15, 0.25 and 0.3), directing to investigate the structural, microstructural and magnetic properties of the prepared perovskites.

2. Experimental details

2.1. Material and methods

The polycrystalline monophase $La_{1-x}Y_xFeO_3$, (x= 0.00, 0.05, 0.1, 0.15, 0.25 and 0.30) were prepared using citrate-nitrate auto-combustion method. The reagent were $La(NO)_3{\cdot}6H_2O$ (Alfa Aesar, 99.99%), $Fe(NO_3)_3{\cdot}9H_2O$ (Alfa Aesar, 99.98%),$Y(NO_3)_3.6H_2O$ (Alfa Aesar, 99.9%) and citric acid monohydrate $C_6H_8O_7{\cdot}H_2O$ (Alfa Aesar, <99.5%). The metal nitrates were separately dissolved in distilled water for 1 hour and mixed together under continuous stirring. The metals to citric ratio were kept at (1:1). The solution was evaporated at a temperature range of 80-100 ^oC with continuous stirring using magnetic stirrer (1650 rpm) and pH controlled by addition of appropriate amount of NH_3 solution (33.3 %) during the stirring process drop wise (PH=7). The prepared samples were obtained by decomposition of the dried gel at a temperature of 300 ^oC in air atmosphere, and finally the bluffly dark yellow powder was gotten after an intense exothermic combustion reaction. The darkness of powder increased by increasing the Yttrium content.

$$La(NO_3)_3{\cdot}6H_2O + Fe(NO_3)_3{\cdot}9H_2O + 2C_6H_8O_7{\cdot}H_2O \xrightarrow{pH=7} LaFeO_3 + 12CO_2 + 2N_2 + 2NO_2 + 25H_2O \quad (1)$$

2.2. Characterization Techniques

The crystal structures of the prepared perovskites were analyzed using synchrotron room temperature XRD. The Synchrotron XRD measurements were executed in transmission mode at MCX beamline of ELETTRA Synchrotron, Trieste, Italy. A beam wavelength of λ = 0.7 Å from Si (111) double-crystal monochromator in non-dispersive arrangement was employed, at 18 m from the source and the focus, and the mirrors positioned symmetrically around it, the diffraction patterns with sample to detector distance of 120 mm. Two dimensional powder diffraction data were transformed into one dimensional pattern (2θ versus intensity) by employing Fit2D. The Instrumental Profile Function of MCX was experimentally determined analyzing the LaB_6 line profile standard, using borosilicate glass capillaries (0.3 mm diameter) in the traditional Debye-Scherrer geometry. The optics of the beamline produce X-rays with energy between 4 and 21 keV. Lattice parameters were determined for each perovskite composition by means of the Rietveld method [12-14].The Rietveld refinement of the room temperature synchrotron XRD patterns was analyzed using the FullProf program. The background was defined choosing several points from the data which were refined simultaneously with other structural parameters. For all the orthoferrite samples under investigation, the refinement procedures were initiated with crystallographic data of $LaFeO_3$ [15]. In this way, lattice parameters, atomic coordinates, thermal parameters, occupancies and microstructural parameters were refined for the whole samples. In the structural analysis, an asymmetric Thompson-Cox-Hastings pseudo-Voigt function was used to describe the peak shapes for different samples. GFourier program (FullProf package) was used for the calculation and visualization of

electron density within the unit cell. Williamson-Hall plot was used to calculate the crystallite size and microstrain based on the refinement of synchrotron XRD.A full explanation of the mathematical processes performed in the Rietveld analysis has been described later elsewhere [16-23].

Magnetizations (M) at room temperature as a function of applied field (H) for the prepared orthoferrites were performed by a VSM (Lakeshore 7310, ACR, El-Dokki, Egypt) in an applied magnetic field between +20 and -20kOe.

The shape, morphology and electron diffraction of the prepared orthoferrites powder were evaluated and analyzed using high-resolution transmission electron microscopy (HRTEM, JEOI-JEM 2100 instrument, National Research Center (NRC), El-Dokki, Egypt).

3. Results and discussion

3.1. XRD analysis

Figure 1 shows the room temperature synchrotron XRD patterns of the series of perovskite $La_{1-x}Y_xFeO_3$, (X = 0.00, 0.05, 0.1, 0.15, 0.25 and 0.30) synthesized through the citrate auto-combustion route. The formation and completion of the reaction is confirmed by the absence of reactants' peaks and the formation of the corresponding perovskite. Peaks corresponding to the (101), (121), (220), (202) and (123)planes were detected, confirming the formation of a pure $LaFeO_3$phase with a well-defined orthorhombic structure (SG Pnma (62), coinciding with JCPDS: 88-0641)without any impurity phase. A shifting towards higher 2θ values with Y content is observed because of the smaller size of Y^{3+} cation compared to La^{3+} cation. [24].

The crystallite size and microstrain for the samples under investigation were calculated using Williamson-Hall method. Strain-induced broadening arising from crystal imperfections and distortion are related by

$$\varepsilon = \frac{\beta_s}{\tan\theta} \qquad (2)$$

The different methods presented in the following assume that size and strain broadening are additive components of the total integral breadth of a Bragg peak [25]. The distinct θ dependencies of both effects laid the basis for the separation of size and strain broadening in the analysis of the Williamson – Hall, as in the following equations:

$$\beta_{hkl} = \beta_\varepsilon + \beta_D = \left(\frac{K\lambda}{D\cos\theta}\right) + (4\,\varepsilon\tan\theta) \qquad (3)$$

$$\beta_{hkl}\cos\theta = \left(\frac{K\lambda}{D}\right) + (4\,\varepsilon\sin\theta) \qquad (4)$$

The strain was expected to be isotropic, where all the material characteristics are independent of the direction along which they are measured. The term ($\beta_{hkl}\cos\theta$) was plotted against (4 sinθ) for the refined synchrotron XRD data of orthorhombic provskites $La_{1-x}Y_xFeO_3$, (X=0.0, 0.05, 0.1, 0.25 and 0.3), the strain component was calculated from the slope (ε) and the average crystallite size component from the intercept (Kλ/D), see figures2 (a-e). The estimated particle size of the as-prepared samples varies from 18 nm to 27.8 nm.

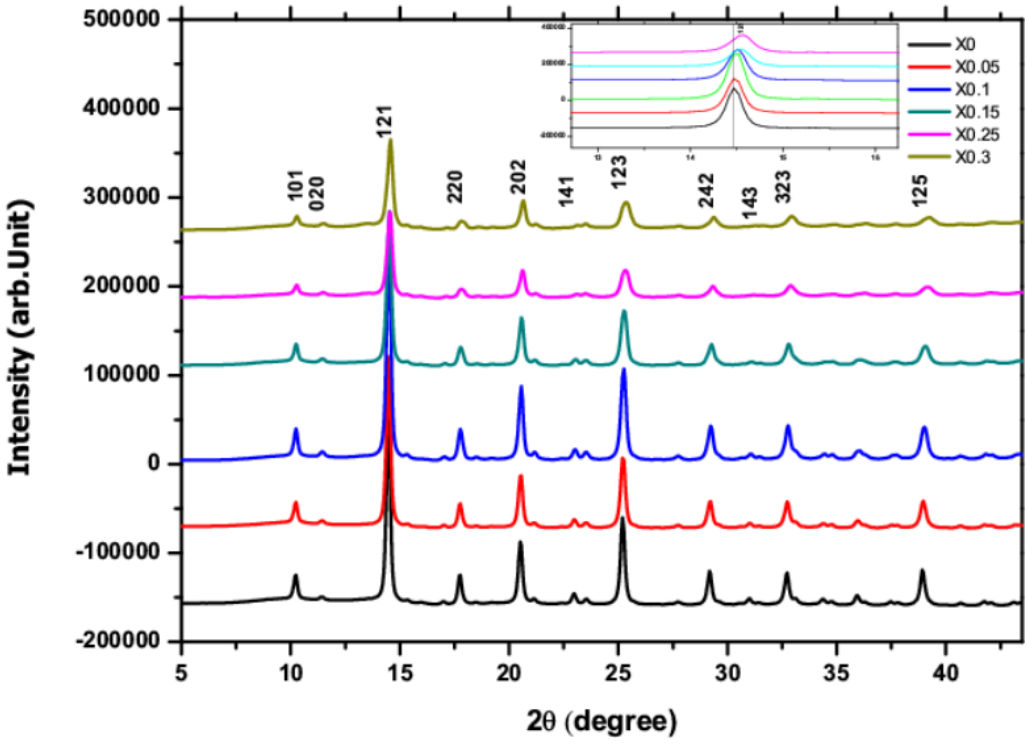

Figure 1. The room temperature synchrotron XRD patterns for multiferroic $La_{1-x}Y_xFeO_3$, (X=0.00, 0.05, 0.01, 0.15, 0.25 and 0.3).

Goldschmidt's tolerance factor is an indicator for the stability and distortion of crystal structures [26].The Goldschmidt tolerance is calculated from the ratio of the ionic radii, and given from formula:

$$t = \frac{R_o + R_A}{\sqrt{2}(R_o + R_B)} \qquad (5)$$

Where, R_A, R_B and R_O are the ionic radii of the A and B site cations and oxygen anion, respectively.If the A cation is smaller than the ideal value, then Goldschmidt's tolerance factor will be smaller than 1. As a result the [BO_6] octahedra will tilt in order to fill space. The perovskite structure is stable in the range (0.75 < t <1.0), and is cubic at (t >0.95) [27], for ideal cubic structure (t=1).

La^{3+} and Y^{3+} ionic radii are 1.16 Å and 1.019 Å on 8-fold coordination while that of Fe^{3+} and O^{2-} are (0.55Å and 1.42Å) respectively on 6-fold coordination. The values of tolerance factor in the range of (0.85 < t < 0.95) which assure the orthorhombic structure of the investigated perovskite samples. The values of the tolerance factor decreased with increasing Y content at the expense of La^{3+} due to the difference in the ionic radii of both La^{3+} and Y^{3+} ions, the variation of tolerance factor with Y content is shown in figure 3. This increases in distortion originated from tilting of <FeO_6> octahedron as a result of increasing the R_B cation size. In other words, the Fe–O–Fe angle changed.

Refinements of the synchrotron XRD data were performed in the SG Pnma for all the prepared samples. The Rietveld plots of the refinements for the prepared orthoferrite system $La_{1-x}Y_xFeO_3$ are presented in Figures 4(a-e).

Lattice parameters of the orthoferrites samples were refined for all the compositions, and the results are displayed in Table 1. A comparison between the five orthorhombic orthoferrites reveals that substitution with

Y produces a significant decrease of the unit cell volume, which is an expectable result due to the smaller size of Y^{3+} cation with respect to La^{3+}. However, the lattice reduction is not isotropic: lattice parameters b and c undergo a slight decrease while the lattice parameter a shows a slight increase, indicating a noticeable distortion of the lattice geometry as the yttrium content increases. Figure 5 summarizes these observations.

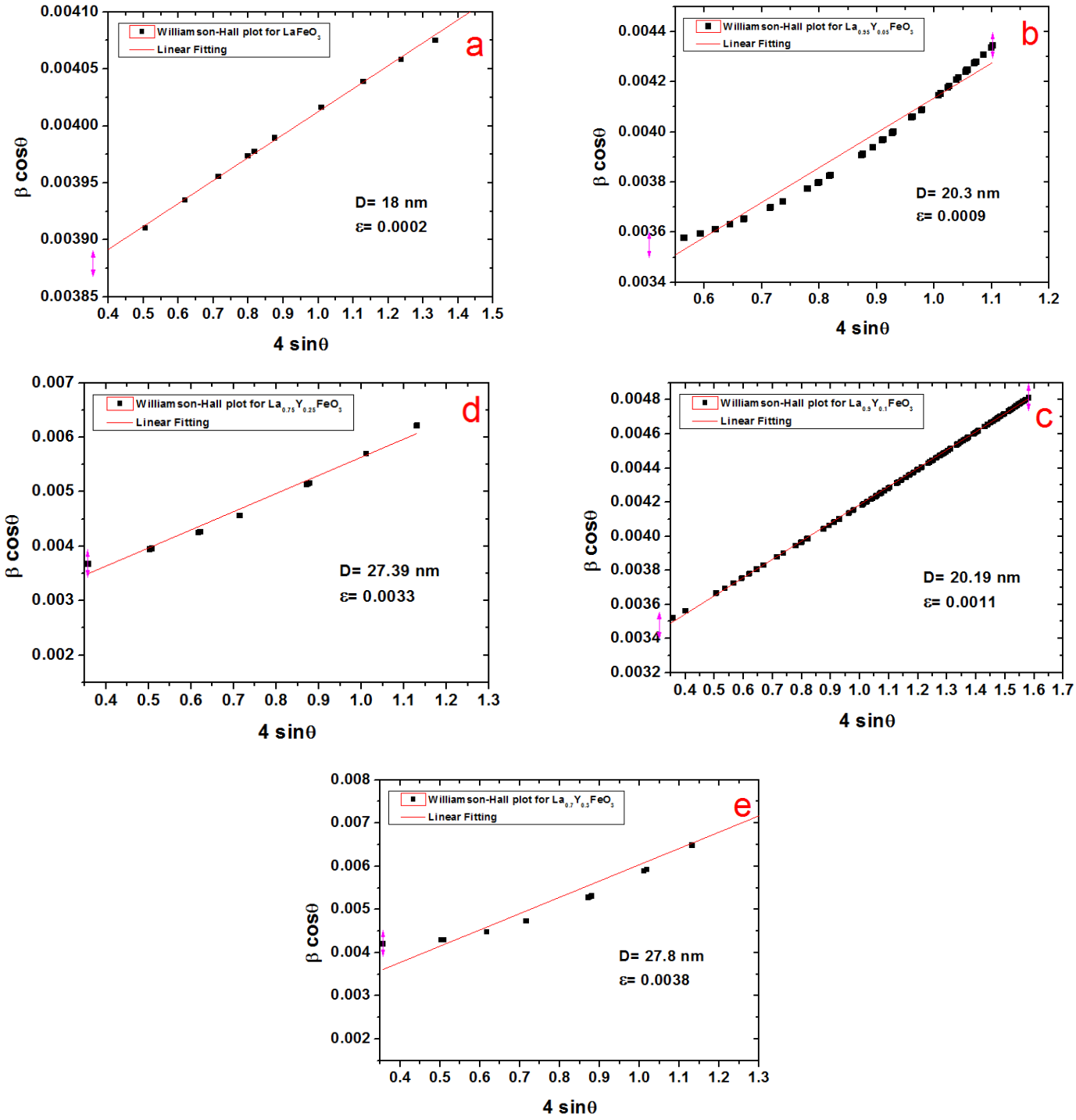

Figure 2. Williamson-Hall Plot for (a) perovskite $LaFeO_3$ (b)$La_{0.95}Y_{0.05}FeO_3$

(c) $La_{0.9}Y_{0.1}FeO_3$ (d) $La_{0.75}Y_{0.25}FeO_3$ (e) $La_{0.70}Y_{0.3}FeO_3$

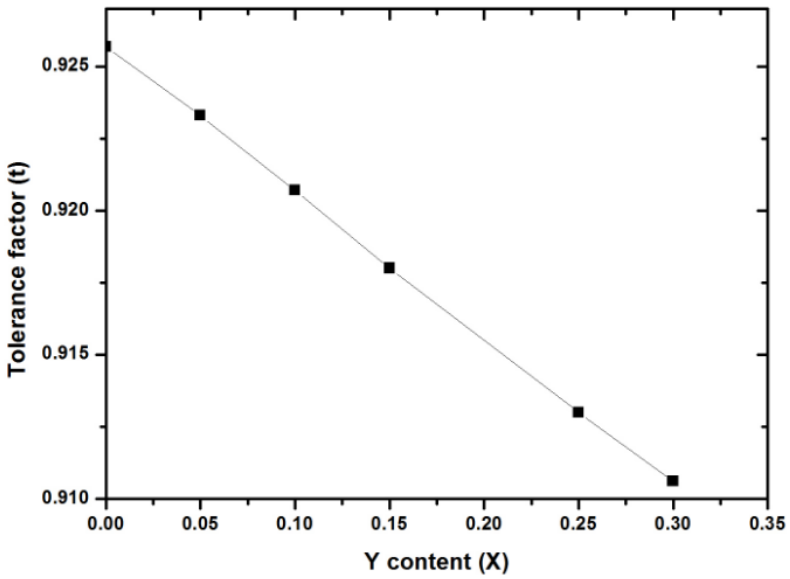

Figure 3.The variation of the tolerance factor with Y content (x).

Among the significant results achieved by Rietveld refinement include electron density mapping using (GFourier program), which used to characterize and visualize the electron density within the unit cell. The visualization is important in recognizing the atomic positions of constituent elements within the unit cell for known or unknown crystals, i.e. thicker the electron density contours show the position of a heavier element among the main elements in the unit cell. The scattering density ρ(x,y,z) is typically calculated according to the equation:

$$\rho(x,y,z) = \frac{1}{V}\sum_{hkl}\left|F_{(hkl)}\right|e^{\{-2\pi i\,(hx+ky+lz-\alpha_{hkl})\}} \qquad (6)$$

Where (x,y,z) is the electron density at a point x,y,z in a unit cell of volume V, F(hkl) is the amplitude of structure factor and α_{hkl} is the phase angle of each Bragg reflection.

Electron density maps may then be displayed as either a 2-D or 3-D Fourier map.Two-dimensional maps are classically drawn with contours (and sometimes color) to show different density levels, while three-dimensional maps employ a chicken-wire style mesh indicating a single level. The 2-D maps of the multiferroic$La_{1-x}Y_xFeO_3$ are shown in Figures 6(a-d).The zero-level density contour is shown in black, but the colored regions of red to violet-brown indicate increasing in levels of electron density around the La cation. Moderately large displacements in the various oxygen positions in the unit cell are detected compared to the Fe and La⎪Y positions, where strong positive peaks correspond to the 4c sites. In the multiferroic system under investigation, the cations Fe and La are located at (0, 0, 0.5) and (0.028, 0.25, 0.993) respectively. The difference in the scattering density between the oxygen anion and La⎪Y and Fe cations is very marked and revealed in Figures 6(a-d).

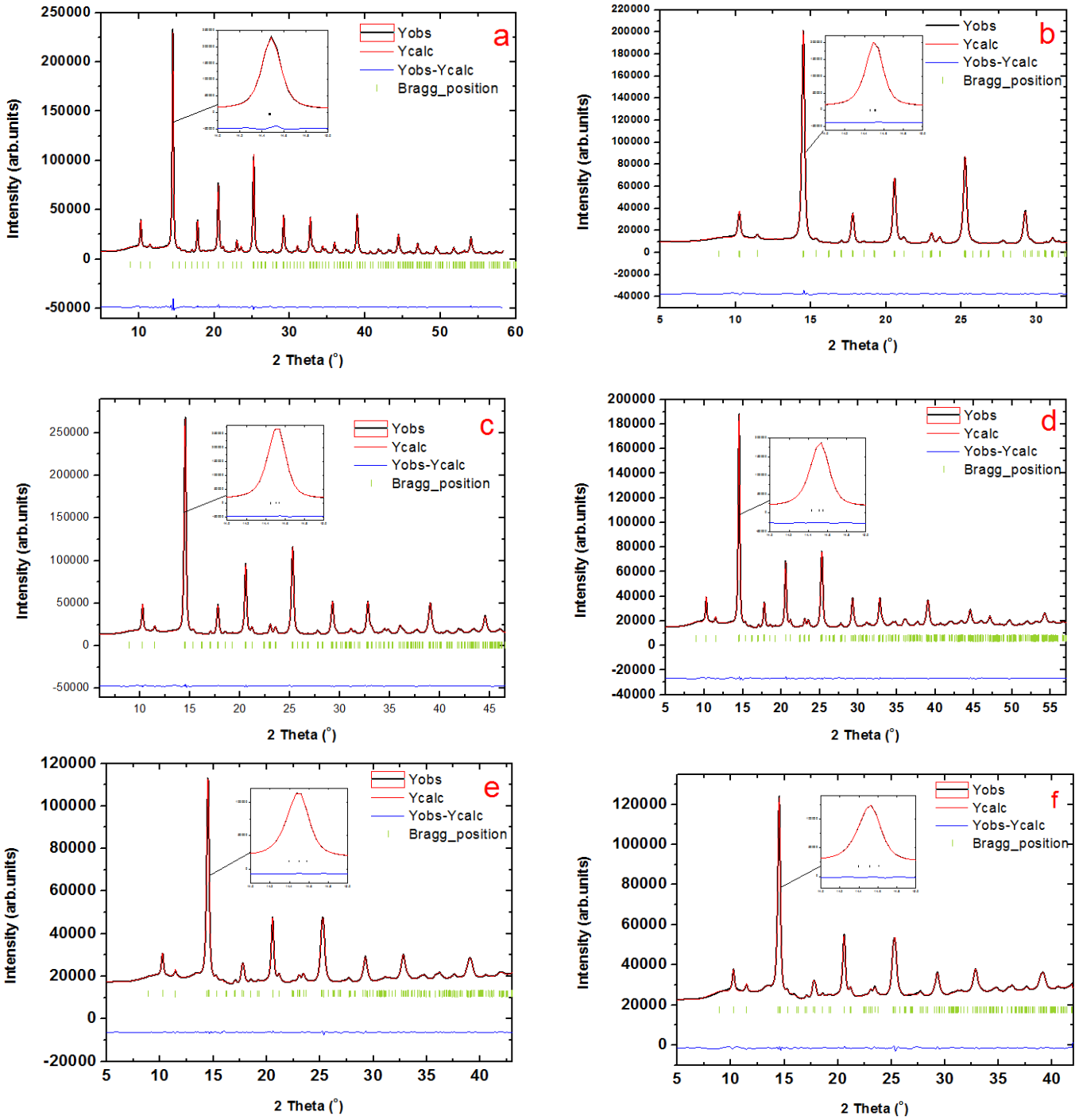

Figure 4.The profile fitting for (a) The orthoferrite $LaFeO_3$ (b) $La_{0.95}Y_{0.05}FeO_3$

(c) $La_{0.9}Y_{0.1}FeO_3$ (d) $La_{0.85}Y_{0.15}FeO_3$ (e) $La_{0.75}Y_{0.25}FeO_3$ (f) $La_{0.70}Y_{0.3}FeO_3$

Table 1.Structural parameters [the lattice parameters (a, b, c), the unit cell volume (V), the particle size (D_{XRD}), Rietveld refinement parameters and the tolerance factor (t)], of multiferroic system $L_{1-x}Y_xFeO_3$.

Y content (x)	Lattice parameter				Refinement parameters					D_{XRD} (nm)	Tolerance factor (t)
	a (Å)	b (Å)	c (Å)	V(Å)	R_{wp}	R_{exp}	R_P	R-factor	χ^2		
0.00	5.5540	7.8443	5.5479	241.706	2.53	1.53	2.31	2.75	2.05	18.0	0.926
0.05	5.5617	7.8350	5.5406	241.437	3.72	1.61	3.80	1.18	2.01	20.3	0.923
0.10	5.5673	7.8349	5.5333	241.358	3.27	1.59	3.61	1.14	2.04	23.9	0.920
0.15	5.5719	7.8309	5.5256	241.098	3.98	2.30	3.45	2.00	2.00	26.2	0.918
0.25	5.5775	7.8302	5.5171	240.948	2.80	2.79	3.43	0.97	1.00	37.5	0.913
0.30	5.5866	7.8283	5.5055	240.775	4.40	2.89	5.90	1.50	2.00	34.5	0.910

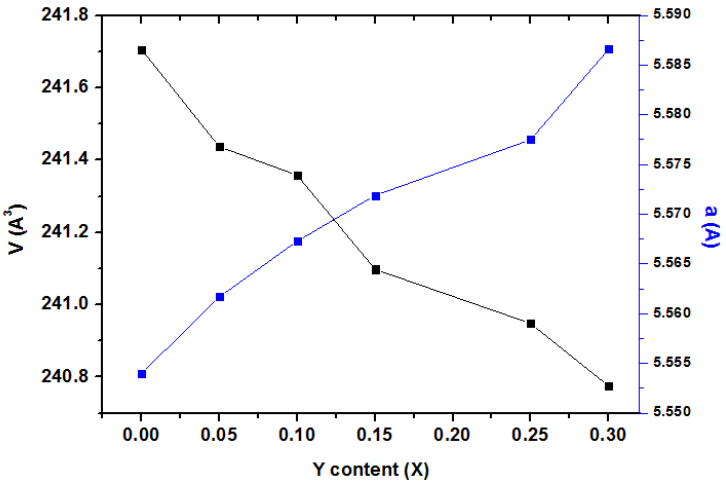

Figure 5.Variation of lattice parameter (a) and volume (V) as a function of Y Content (X) for multiferroic system $La_{1-x}Y_xFeO_3$.

Figure 7 demonstrates a 3-D Fourier map of individual atoms in the unit cell of $La_{0.75}Y_{0.25}FeO_3$, at X=0. The strong positive peaks corresponding to the 4c sites for La|Y cations (A-site). Some intermediate nuclear density is observed between both peaks related to the 4b sites for Fe^{3+} cation (B-site).

Perovskites has been classified by Glazer (1972; 1975) based on tilting of octahedra and has suggested that the total symmetry follows that of the tilts in spite of displacements and distortions. It is intended that the alternative definition of tilt angles used here is sufficient to calculate the polyhedral volume ratio, VA/VB,

but not to regenerate the coordinates of all ions unambiguously. The parameterization to be developed here can also take octahedral irregularities into account, as the values of the tilt angles in $LaFeO_3$ are derived from computational analysis of experimental structural data. Figure 8 shows the irregular tilted $[FeO_6]$ octahedral for perovskite $LaFeO_3$.

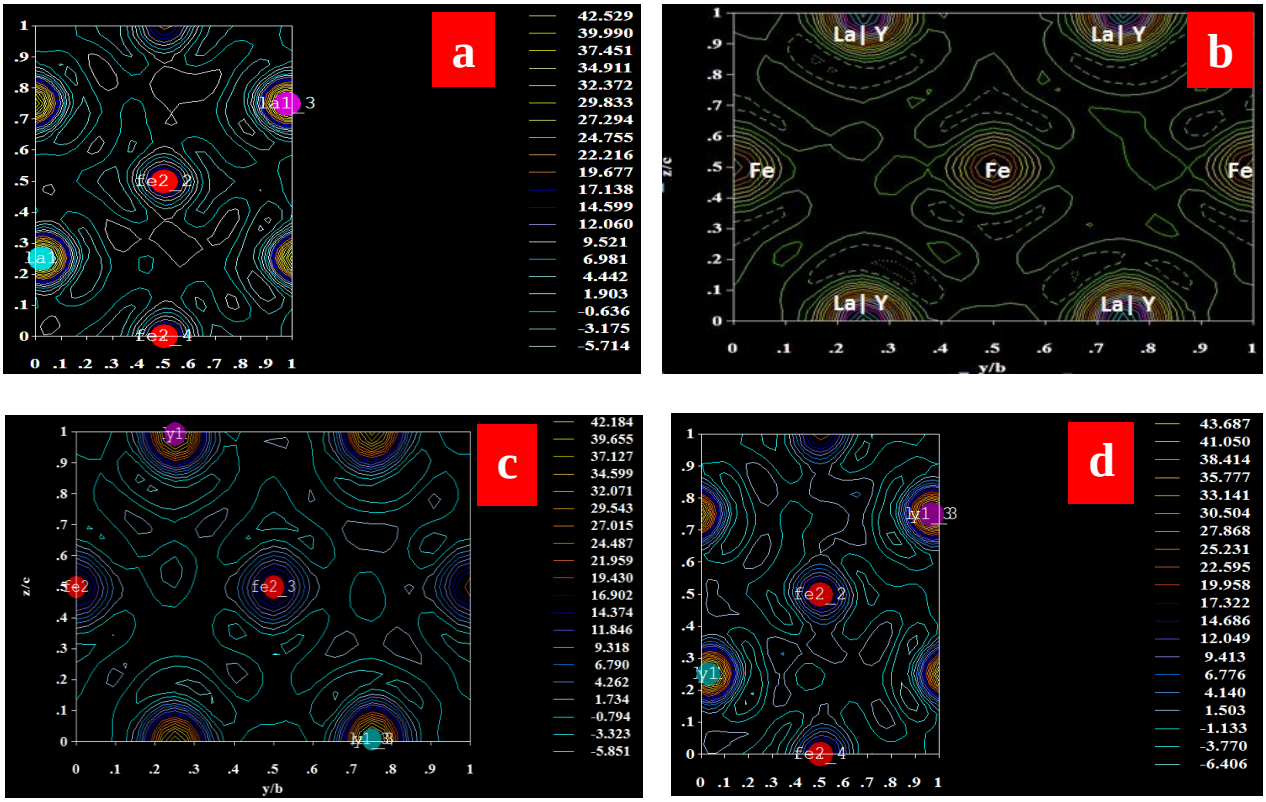

Figures 6(a-d): 2-D Electron density map of individual atoms on xy plane in the unit cell of (a) perovskite $LaFeO_3$ (b) $La_{0.85}Y_{0.15}FeO_3$ (c) $La_{0.75}Y_{0.25}FeO_3$ (d) $La_{0.7}Y_{0.3}FeO_3$, the electron density is measured in electrons per cubic angstrom, e $Å^{-3}$.

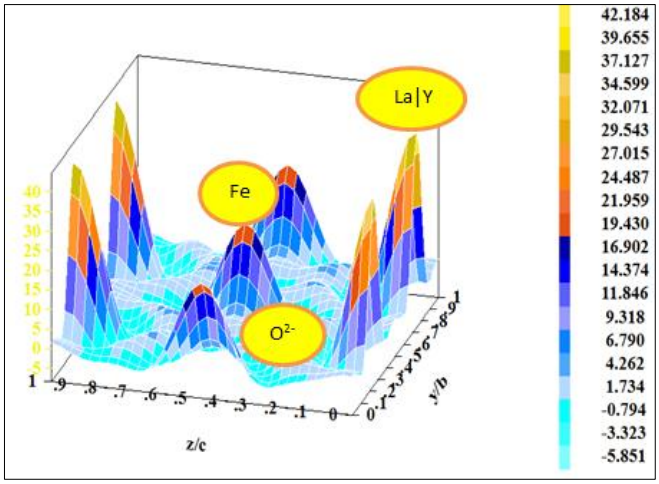

Figure 7. 3D- Electron density map of individual atoms in the unit cell of $La_{0.75}Y_{0.25}FeO_3$, at X=0, La|Y peak is clearly located on 4c sites; the electron density is measured in electrons per cubic angstrom, e $Å^{-3}$.

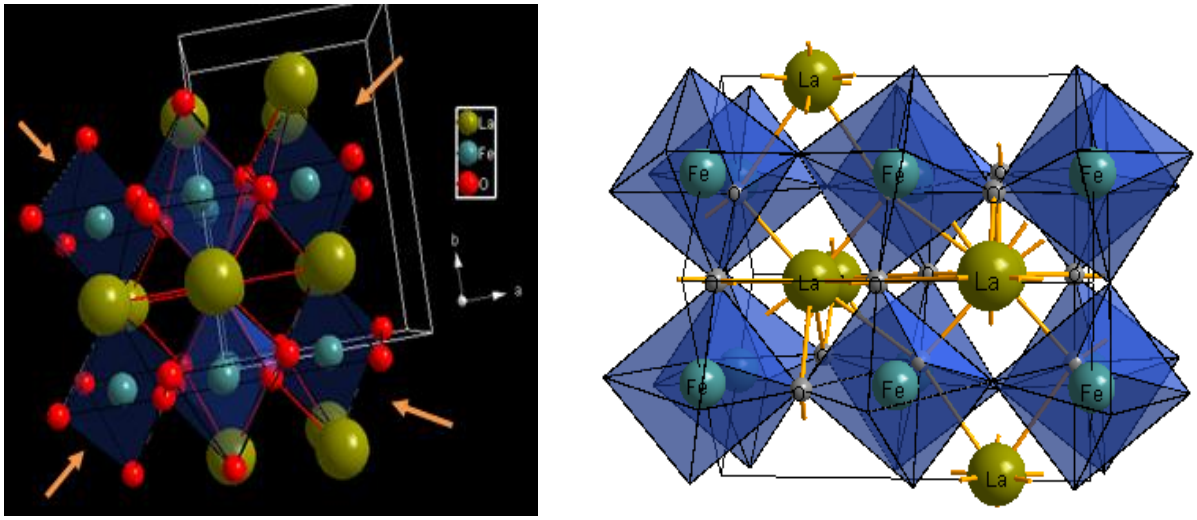

Figure 8. The irregular tilted octahedral [FeO_6] for perovskite $LaFeO_3$.

3.2. Magnetic Measurements

The M(H) hysteresis loops of the prepared $La_{1-x}Y_xFeO_3$multiferroic system were measured at room temperature by VSM in the field varies between +20 kOe to -20 kOe. The magnetizations of samples were measured by a VSM in a field of 15 kOe from 500 to 800 K. The Curie temperature for $LaFeO_3$, $La_{0.9}Y_{0.1}FeO_3$ and $La_{0.7}Y_{0.3}FeO_3$were determined by the M(T) curve, as displayed in Figure 9.The Curie temperature was dropped from 730 K for $LaFeO_3$to approximately 710 K for $La_{0.7}Y_{0.3}FeO_3$.The M(H) hysteresis loops for the orthoferrite system $La_{1-x}Y_xFeO_3$are shown in Figure 10.

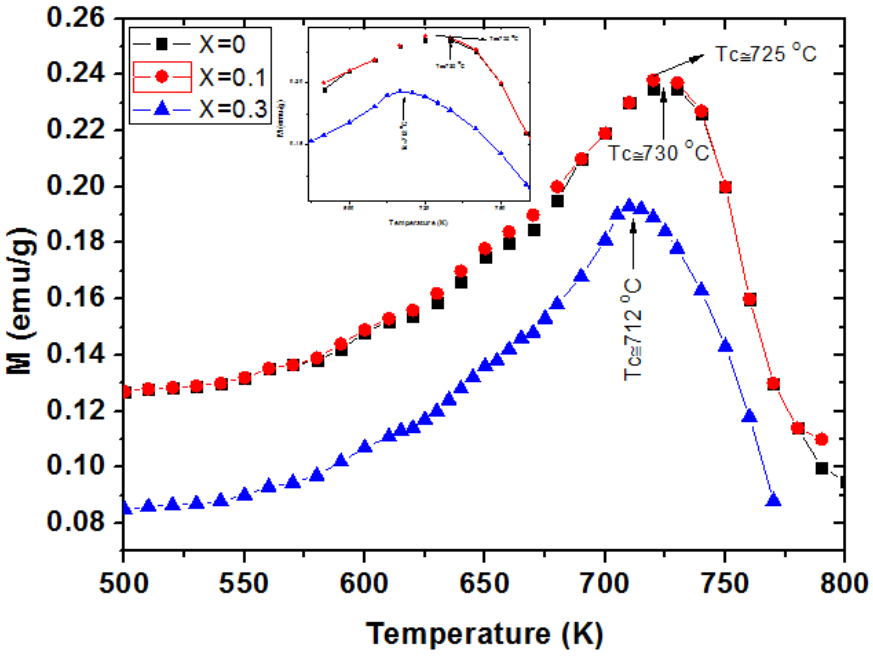

Figure 9. The M(T) curves for the prepared $LaFeO_3$, $La_{0.9}Y_{0.1}FeO_3$and $La_{0.7}Y_{0.3}FeO_3$.

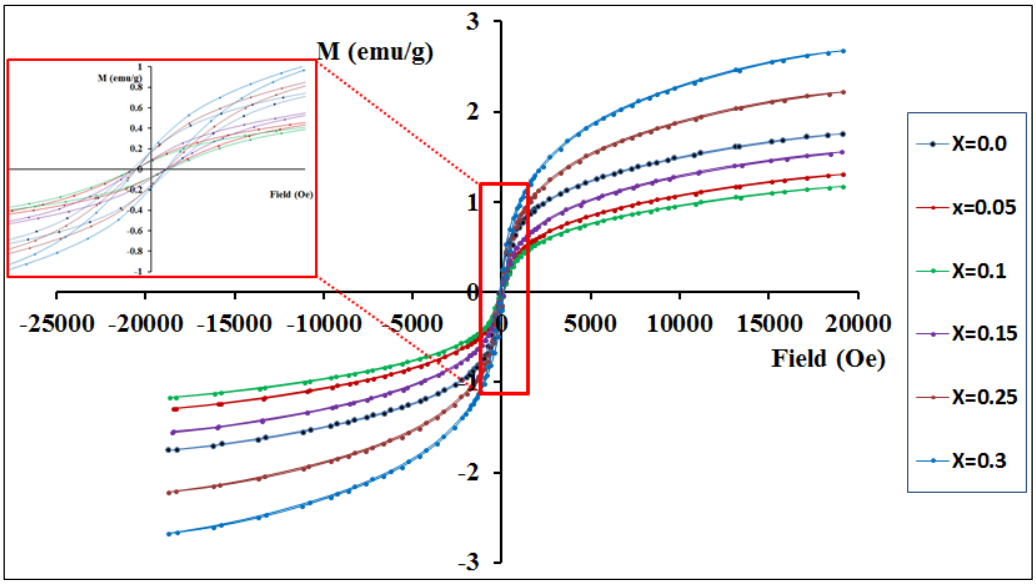

Figure 10.Room-temperature M(H) curve of prepared perovskite system $La_{1-x}Y_xFeO_3$, (X=0.0, 0.05, 0.1, 0.15, 0.25 and 0.3) in the field range of ±20 KOe.

The $LaFeO_3$ perovskite is known to show antiferromagnetic nature at room temperature, as mentioned before [28]. Conversely, the M(T) and M(H) curves of the prepared perovskite show weak ferromagnetic behavior. The M(H)curve for pure $LaFeO_3$ perovskite confirms weak ferromagnetic character with the maximum magnetization (M) at 20 kOe of ~1.76 emu/g and H_C of ~125 Oe. The lowest magnetization for perovskite $La_{0.9}Y_{0.1}FeO_3$ at 20 kOe of ~1.17 emu/g and increased up to 2.68 emu/g for $La_{0.7}Y_{0.3}FeO_3$, see Table 2. This might be affected by antiferromagnetic ordering with canted spins [29]. Therefore, the room-temperature ferromagnetism in the investigated samples can be described by the supper exchange (SE) interaction of the Fe^{3+}–O^{2-}–Fe^{3+} ions, that induces a ferromagnetic shell model at the particle surface due to disordered spins, however an antiferromagnetic core is induced due to ordered spins [30,31]. This behavior indicated an increasing ratio of the volume fractions of disordered spins to ordered spins of the Fe^{3+} ions with a decreasing crystallite size, as well as a great surface area, ensuing in an increased magnetic interaction. The hysteresis loop parameters obtained from VSM for the perovskite system $La_{1-x}Y_xFeO_3$ are presented in Table 2. Additionally, during heating of the samples, some coupling Fe^{3+}-Fe^{2+}ions may appear caused by the oxygen loss [32]. The contribution of magnetic behavior of the as prepared perovskitedue to the difference between the magnetic moments of the Fe^{3+}(5 μ_B) and Fe^{2+} ions (4 μ_B).

Table 2. Magnetic parameters calculated from M (H) curve for the prepared orthoferrites.

Y content (X)	Hci (Oe)	Ms(emu/g)	Mr(emu/g)	RetentivityMr (emu/g)	R=Mr/Ms	H_{C+} (Oe)	H_{C-} (Oe)	H_{EX} (Oe)
X=0.00	125.03	1.7566	0.16687	0.1687	0.095	125.03	124.99	0.020
X=0.05	103.53	1.2993	0.08152	0.0782	0.063	100.45	106.62	3.058
X=0.10	111.98	1.1716	0.07900	0.0771	0.067	111.89	112.07	0.090
X=0.15	94.49	1.5554	0.09191	0.0893	0.059	94.131	94.848	0.358
X=0.25	99.896	2.2195	0.15494	0.15277	0.069	99.915	99.877	0.019
X=0.30	95.787	2.6780	0.17809	0.17781	0.066	95.783	95.791	0.004

If the prepared powder has some multiple domain sizes particles, Hc, Mr, and squareness ratio R will diverge from zero. A larger particle size will provide a higher R value with a more apparent ferromagnetic behavior. Thus, we suggested that the ratio R = Mr/Ms could be used as a parameter to measure the homogeneity on the nanoparticle dimensions and the maximum limit of the single domain size of the magnetic nano-sized powder material. As stated above, the prepared nano-sized powders are weakly ferromagnetic, which shows that Mr≠ 0. These materials are consisting of single-domain and multiple-domain particles. The magnetization of samples is considered as the summation of two terms:

$$M(H) = M^{sp}(H) + M^{FM}(H) \quad (7)$$

Where, $M^{sp}(H)$ is the impact of the superparamagnetic (sp) nanoparticles (single domain), and $M^{f}(H)$ is the contribution of the ferromagnetic (FM) nanoparticles (multiple domains).

The magnetization of the superparamagnetic nanoparticles can be calculated from:

$$M(H) = M_S \left[\coth\left(\frac{\mu H}{K_B T}\right) - \frac{K_B T}{\mu H}\right] = M_S\, L\left[\frac{\mu H}{K_B T}\right], \quad (8)$$

Where, Ms=Nμ is the saturation magnetization for N nanoparticles with magnetic moment μ [33].The magnetization of the superparamagnetic (sp) phase of the$LaFeO_3$ nanoparticles is given by the formula:

$$M^{sp}(H) = M^{sp}(\infty) \sum_j f\left(\mu_j\right) L\left[\frac{\mu_j H}{K_B T}\right] \quad (9)$$

Where, μ_j is the magnetic moment corresponds to the magnetic moment per atom, and $f(\mu_j)$ is the weighted term of the Langevin function [33]. The magnetic moment (μ) and particle diameter (d) are related by the following relation:

$$\mu = M_S\, d^3\, \pi/6 \quad (10)$$

The particle diameter of the multiferroic system $La_{1-x}Y_xFeO_3$ were calculated by fitting the room temperature M(H) curve based on Langevin function, see Figure 11(a-f).

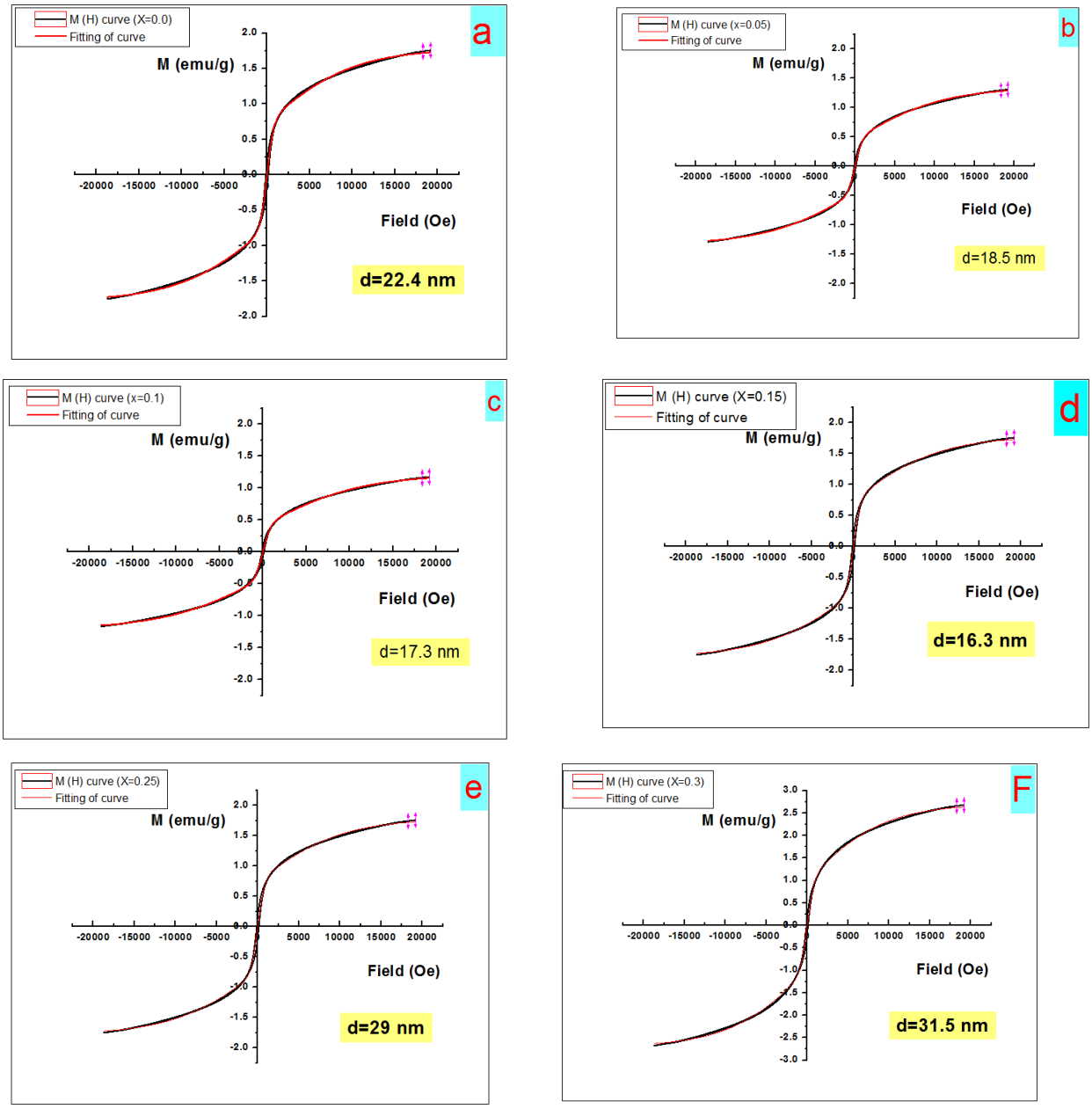

Figure 11.The results of fitting of the Hysteresis curves for (a) orthoferrite $LaFeO_3$ (b) $La_{0.95}Y_{0.05}FeO_3$ (c) $La_{0.9}Y_{0.1}FeO_3$ (d) $La_{0.85}Y_{0.15}FeO_3$ (e) $La_{0.75}Y_{0.25}FeO_3$ (f) $La_{0.70}Y_{0.3}FeO_3$.

Figure 12shows the variation of the inverse molar magnetic susceptibility ($1/\chi_M$) with the absolute temperature at the magnetic field of (1.5 KOe) at a temperature range of (500-850 K) for the orthoferrite samples $LaFeO_3$, $La_{0.9}Y_{0.1}FeO_3$ and $La_{0.7}Y_{0.3}FeO_3$. It is clear that, the values of $1/\chi_M$ increase with temperature. It is possible for appearance some antiferromagnetic phase and even some local magnetic phase separation which results in the decrease of magnetization. The Cuire-Weiss formula was used to analyze the $1/\chi$ versus T curve for the prepared samples, shown in Figure 12(a-c).The susceptibility of the ferromagnetic material frequently obeys the Curie-Weiss law (Van Vleck 1959):

$$\chi = \frac{C}{T-\theta} = \frac{M}{H} = \frac{N_A \mu_{eff}^2 \mu_B^2}{3K_B [T-\theta]} \qquad (11)$$

Where $C = N_A \mu_B^2 \mu_{eff}^2 / 3k_B$ is the Curie constant, N_A is Avogadro number, μ_B is the Bohr Magneton, $\mu_{eff} = \mu_B\, g \sqrt{S(S+1)}$ is the effective magnetic moment, g=2 is the gyromagnetic ratio and S is the magnetic spin, k_B is Boltzmann constant, and θ is paramagnetic Weiss temperature.

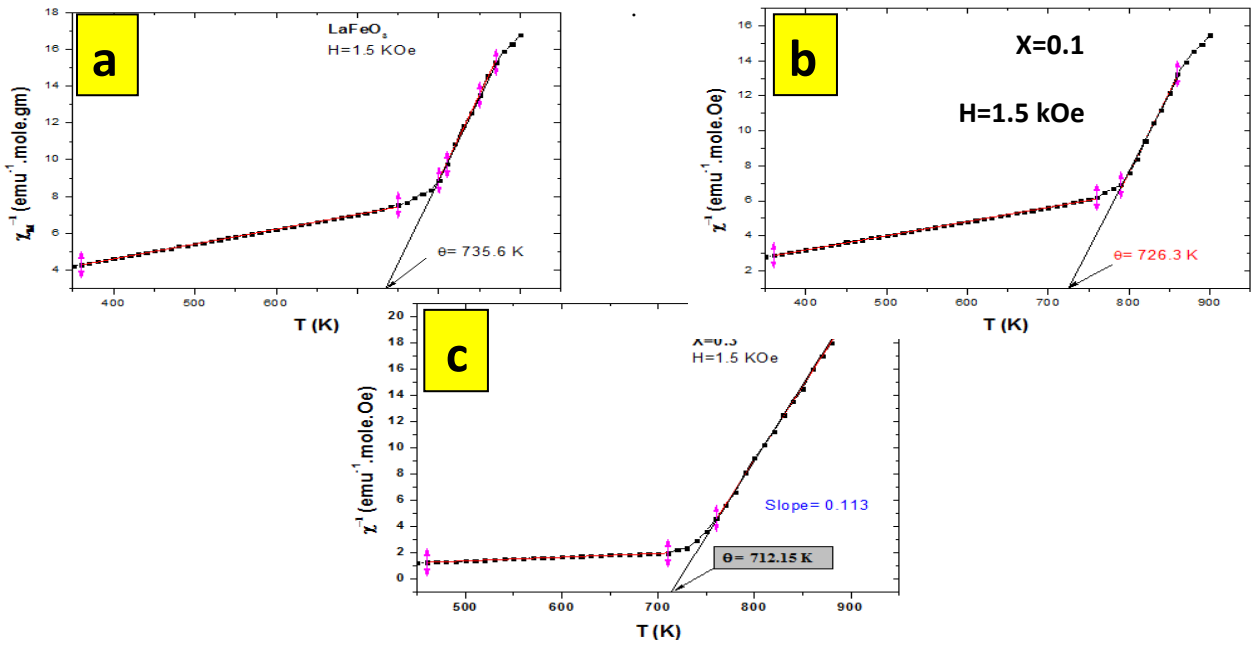

Figure 12. Temperature dependence of inverse molar susceptibility for (a) Perovskite $LaFeO_3$ (b) $La_{0.9}Y_{0.1}FeO_3$ (c) $La_{0.7}Y_{0.3}FeO_3$.

The plots of χ^{-1} vs. T displayed in the Figure 12(a-c) exhibit a linear behavior over the entire range of data. This behavior is characteristic of paramagnetism. The value of the Curie constant is the reciprocal value of the slope and the effective magnetic moment were calculated from:

$$\mu_{eff} = \sqrt{\frac{3\,K_B\,C}{\mu_B N_A}} = 2.83\sqrt{C} \qquad (12)$$

The value of θ is calculated from the intercepting of the straight line with the temperature axis. The data are displayed in Table 3, where θ gives +ve values indicating the ferromagnetic character for the perovskite system.

Table 3. Values of the calculated Curie temperature, Curie constant(C), Curie-Weiss temperature (θ), effective magnetic moment μ_{eff} and the exchange interaction constant (J/k_B) for the prepared perovskite system $La_{1-x}Y_xFeO_3$, (X=0, 0.1 and 0.3).

Y content (x)	C [(e.m.u/g).mol. K]$^{-1}$	μ_{eff} (B.M)	θ (K)	T_c (K)	Jex/ K_B
0.0	10.83	9.31	735.60	730	31.29
0.1	10.78	9.29	726.30	725	31.07
0.3	8.85	8.42	712.15	712	30.43

The exchange coupling between nearest neighbors is resulting in parallel alignment of the magnetizations in ferromagnetic materials. The exchange coupling between nearest spins can be written according to Heisenberg Hamiltonian representation, as follows:

$$Eex = -2J\ SiSj = -2J\ SiSj\ \cos\theta \quad (13)$$

Where J is the exchange integral and S_i and S_j are two neighboring spins. The sign of the exchange integral strength determines whether we have ferromagnetic or antiferromagnetic coupling. For ferromagnetic materials J is positive. The Challenge is to find the way to expose the relationship between the Curie temperature and the exchange integrals for our prepared samples. According to Bethe and Slater [34], when the interatomic distance is small, the electrons spend the majority of their time between the neighboring atoms. This increases the antiparallel alignment and therefore negative J (antiferromagnetic case).

If the atoms are far apart, the electrons spend the majority of their time away from each other so as to minimize the electron repulsions. This leads to parallel alignment or positive exchange J(case of ferromagnetism).

Suppose that, the exchange interaction is effective only over the "Z" is the number of molecules per unit cell, where it takes a value "Jex". The Weiss field theory was used to calculate the exchange integral J_{ex}, from relation, which describe the relation between the Curie temperature T_C and exchange interaction constant J_{ex} in the ferromagnetic case:

$$J_{ex} = \frac{3\ K_B T_C}{2\ Z\ S(S+1)} \quad (14)$$

Where s is the spin (s = 5/2 for Fe^{3+} ion). The values of J_{ex} were represented as J/k_B and reported in Table 3.

The distortion from the ideal perovskite is mainly in the position of the $La^{3+}$and Y^{3+} ions, whereas the Fe^{3+} ions are present in an essentially octahedral environment. Because the alignment of Fe moments is not strictly anti-parallel but slightly canted, this results in a small net magnetization, giving rise to a weak ferromagnetic behavior as we report before. The Dzyaloshinsky–Moriya antisymmetric exchange is the responsible for the canting that reduces a net magnetic moment perpendicular to the uniaxial magnetocrystalline anisotropy. Some researchers [35] discover a mixed action of hard and soft anisotropy fields in a monophase sample of pure $YFeO_3$. But, that doesn't occur for our prepared samples, since the resultant M(H) loop is typical of a single magnetic phase as shown in Figure 10.

When correlating the hysteresis plots with the obtained behavior of $1/\chi_M$ V.s T, which displayed in Figure 12(a-c) and one could argue that a superparamagnetic behavior is obtained, thus, one could explain this trend as: when Y^{3+} ions replace La^{3+} ions, two effects act with each other on the <FeO_6> magnetic sublattice. The first one is the dilution of the magnetic lattice and the transformation of the ferromagnetic order from short range to long range one as the Y content increased. This leads to weakening of the ferromagnetic behavior and then, effective moment has been decreased with increasing Y content as shown in Figure 13. The second one is the decrease of the tilting of the octahedra <FeO_6> with increasing Y content trying to strengthen the ferromagnetic character.

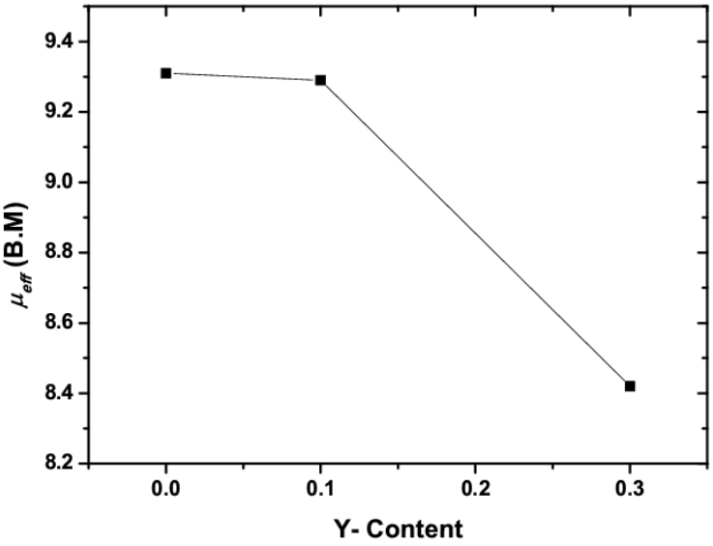

Figure 13.The variation of effective magnetic moment μ_{eff} with Y content for the perovskite system $La_{1-x}Y_xFeO_3$, (X=0.0, 0.1 and 0.3).

3.3. TEM analysis

The structure of the perovskite $La_{1-x}Y_xFeO_3$, (X=0.0, 0.05, 0.10, 0.15, 0.25 and 0.30) nanocrystallites were further analyzed by HRTEM micrographs. According to the XRD results shown in Figure 1, the single phase noncrystalline material consists of many tiny single crystals. Therefore the XRD patterns of the samples under investigation will look like a superposition of single crystal spot patterns and show concentric spotty rings, very close together around the central beam spot. Each ring represents a reflection of the planes family with different interplanar spacing.

Figure 14(a-f) shows the HRTEM images and SAED pattern of the prepared orthoferrite system $La_{1-x}Y_xFeO_3$ nanoparticles. It is clearly that, the particles consisted of an agglomeration of numerous semi-spherical primary particles lightly aggregated together and the unidirectional orientation of the lattice fringes confirmed the polycrystalline character of the prepared orthoferrites. The different values of crystallite diameter investigated by TEM and XRD analysis result from the agglomeration of particles of the prepared samples. The measurement of individual unagglomerated spherical particles is straight forward. However, when nanoparticles are bound together or have an irregular shape for some particles, accurate size statistics can be more complicated to measure. The average particles diameter estimated from the TEM images was about 22nm for $LaFeO_3$ and increased up to 27 nm for $La_{0.7}Y_{0.3}FeO_3$, which were well consistent with that from XRD results.

The HRTEM image of the tip portion of the nanosphere shows the lattice planes with an interplanar spacing of 0.24 and 0.27 nm corresponding to the planes(102) and (121) respectively for compositions $LaFeO_3$ and $La_{0.7}Y_{0.3}FeO_3$ which displayed in Figure 15(a, b) and confirming the XRD analysis. The diffraction rings are discontinuous and consist of sharp spots which show good crystallinity of $LaFeO_3$nanospheres as shown in the SAED pattern in Figure 14(a-f).

The corresponding SAED pattern in the included in Figure 14 indicates its polycrystalline nature, as a result of the diffraction from the nanoparticles. Therefore, by correlating the result of HRTEM profile, it can be concluded that the observed results of TEM confirmed the XRD results, and reitveld analysis.

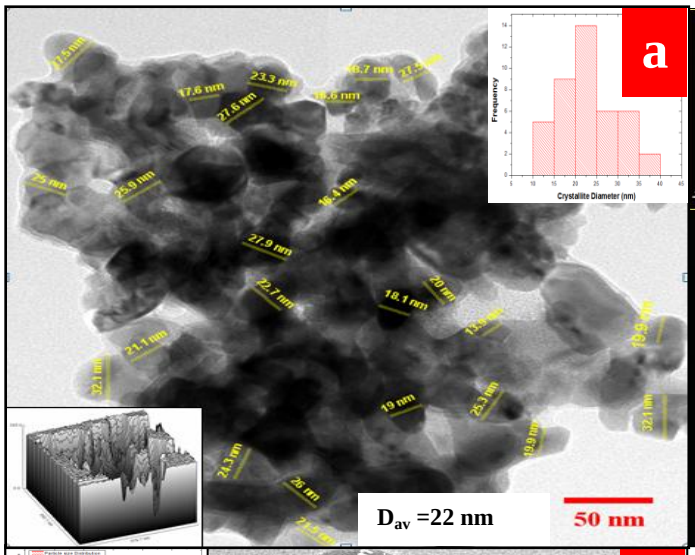
a
Crystallite Diameter (nm)
Frequency
D$_{av}$ =22 nm
50 nm

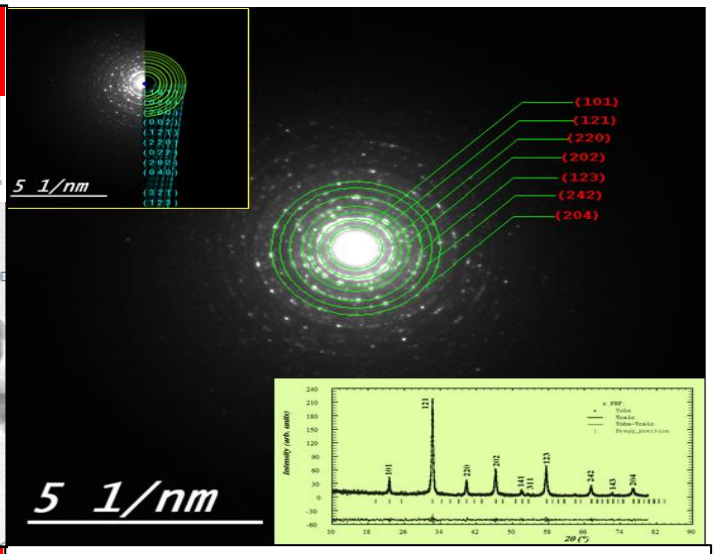
5 1/nm
(101)
(121)
(220)
(202)
(123)
(242)
(204)

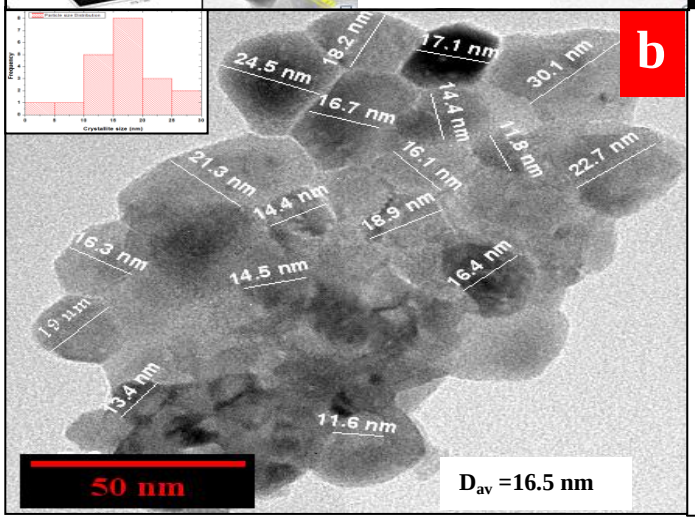
b
50 nm
D$_{av}$ =16.5 nm

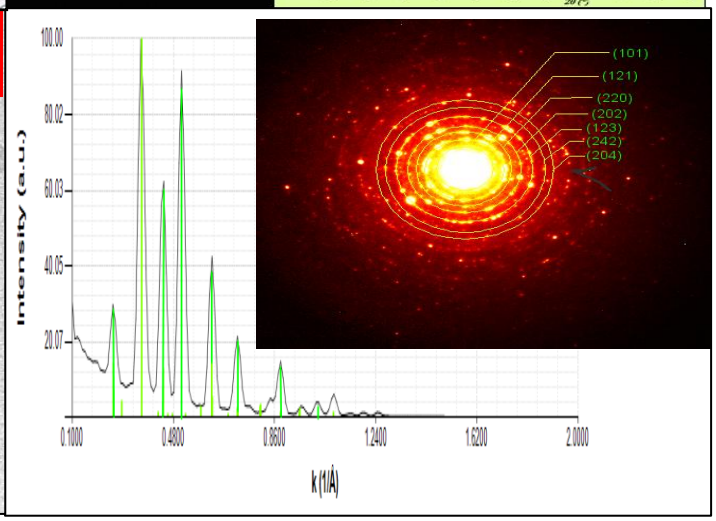
Intensity (a.u.)
k (1/Å)
(101)
(121)
(220)
(202)
(123)
(242)
(204)

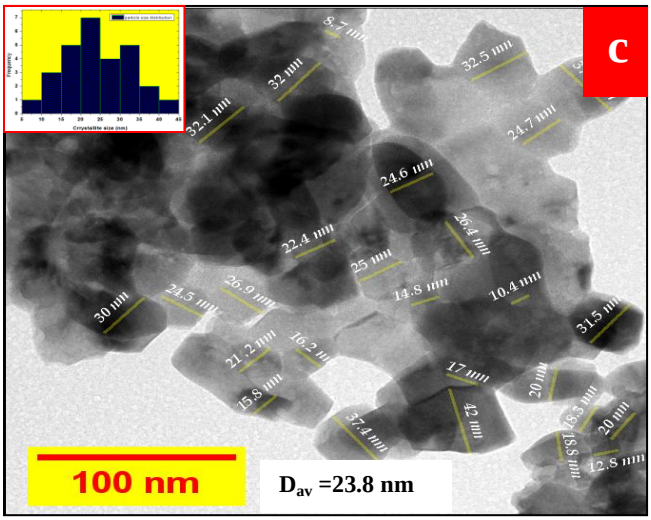
c
100 nm
D$_{av}$ =23.8 nm

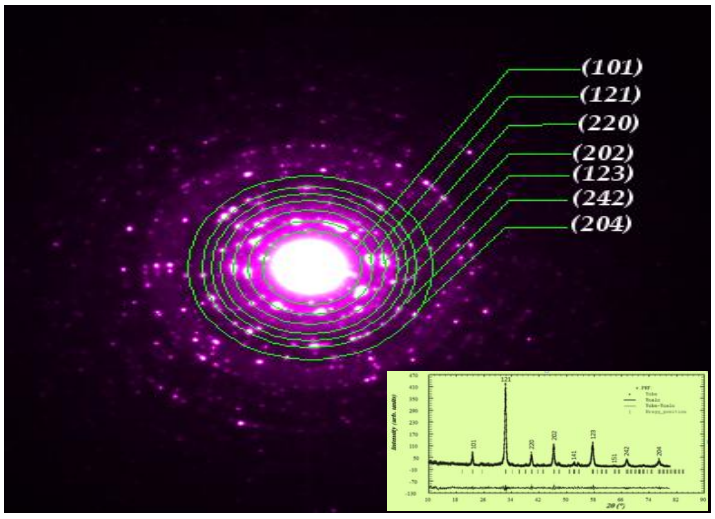
(101)
(121)
(220)
(202)
(123)
(242)
(204)

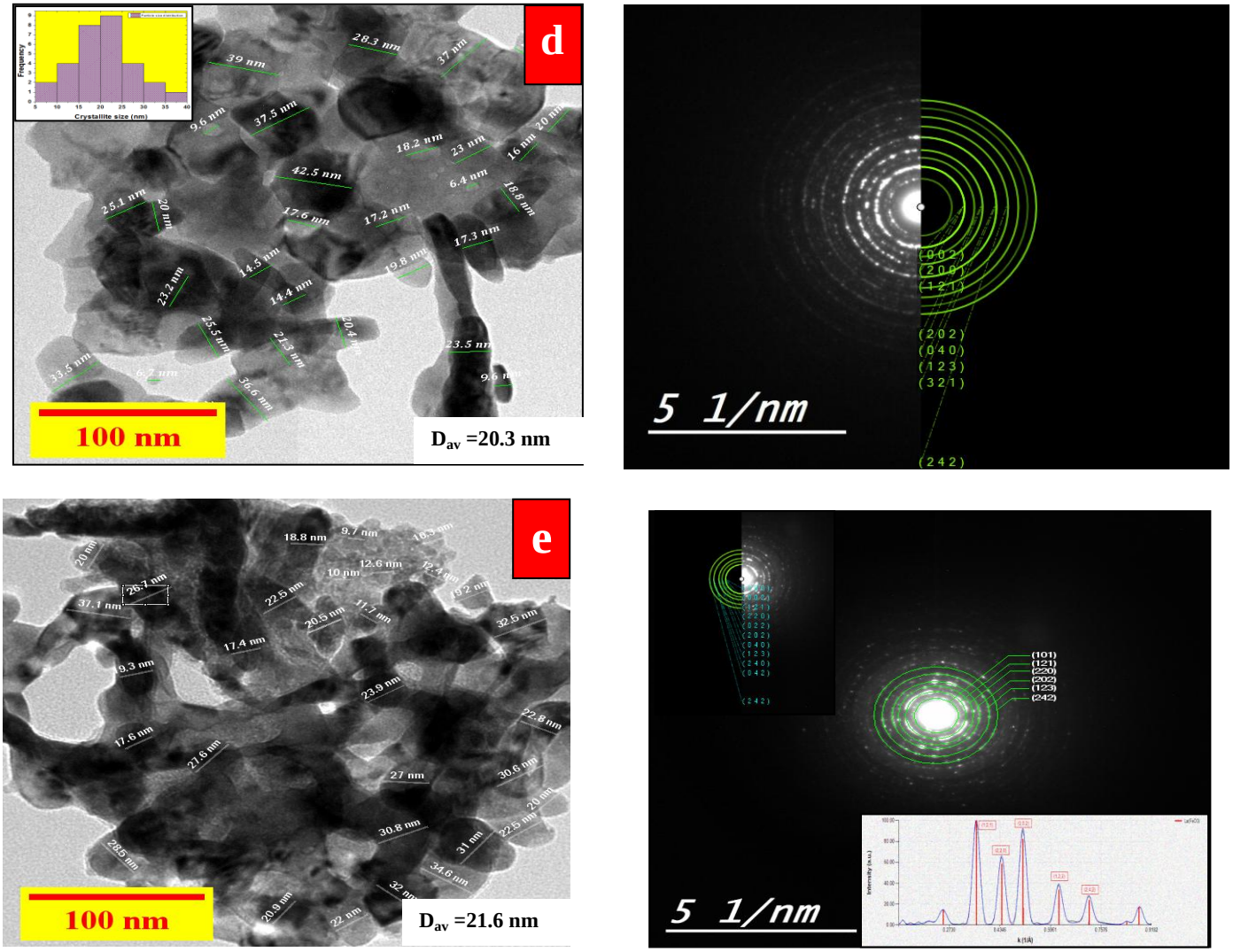

Figure 14.HRTEM images and SAED pattern of (a) perovskite $LaFeO_3$nanoparticles, (b) $La_{0.95}Y_{0.05}FeO_3$(c) $La_{0.9}Y_{0.1}FeO_3$, (d) $La_{0.85}Y_{0.15}FeO_3$, (e) $La_{0.75}Y_{0.25}FeO_3$.

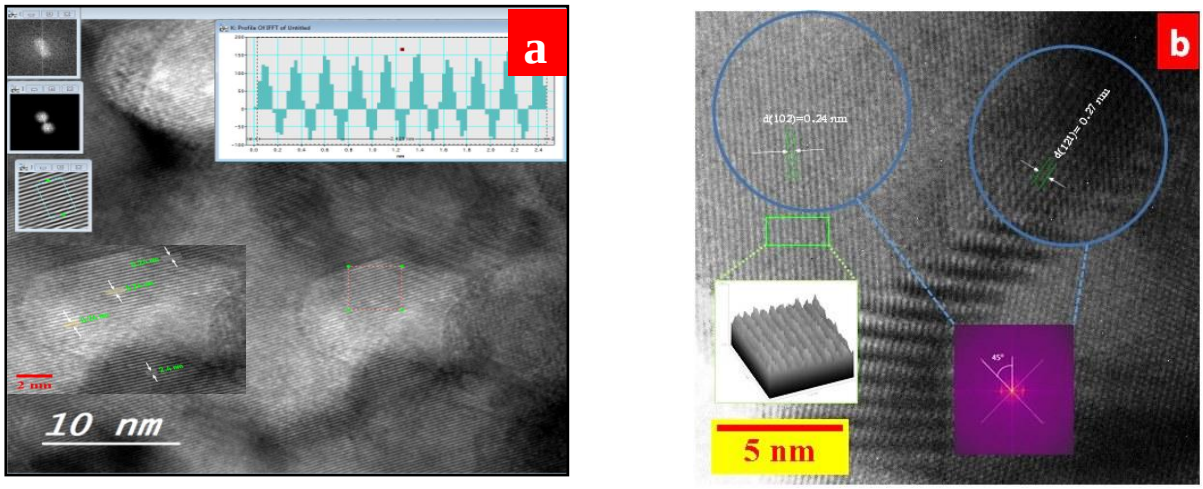

Figure 15. Fast Fourier Transformation (FFT) patterns box to measure the interplanar spacing in the orthoferrite (a) $LaFeO_3$ (b) $La_{0.7}Y_{0.3}FeO_3$.

The major diffraction spots correspond to (101), (121), (220), (202) and (123) of nanosynthesized compositions with an orthorhombic structure (SG: Pnma), without any spot related to any impure phases, and consistent with synchrotron XRD results. The $LaFeO_3$patterns have been indexed using (C spot Trial, version 2.0), see Figure 16. The diffraction profiles created from ring diffraction patterns can be viewed as equivalents of XRD pattern. The FFT patterns for HR-TEM of the perovskite $La_{0.7}Y_{0.3}FeO_3$, corresponding to (121) and (111) plane and show the angle between the two intersecting planes around 90^o, as shown in Figure 17.

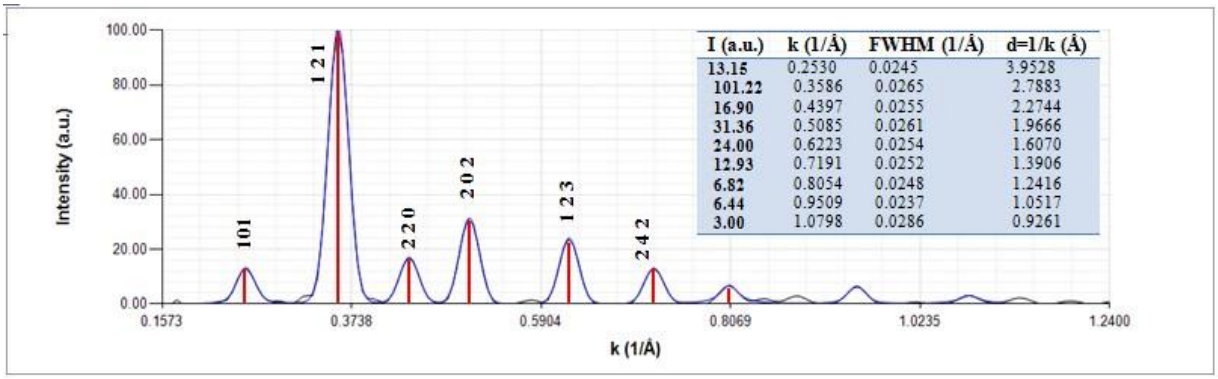

Figure 16. Indexing of SAED patterns for the perovskite $LaFeO_3$, using ''CSpot program''.

Table 4 summarizes and compares the values of these interplanar distances of perovskite $La_{0.75}Y_{0.25}FeO_3$obtained by the XRD and HRTEM measurements.

Intensities of the rings depended on the number of diffracting particles which in turn depended on the size of the selected area. For polycrystalline materials, good diffraction patterns are gotten when the selected area is as large as possible. The crystallites with an area less than 3 pixels were considered as noise since the imaging resolution was about 1nm. The micrograph scale was found to have an error of about 5% above actual measurement.

Table 4. Corresponding interplanar distances for the diffraction peaks (101), (121), (220), (202), (123), (242) and (204) of perovskite $La_{0.75}Y_{0.25}FeO_3$ obtained by synchrotron XRD and HR-TEM techniques.

Diffraction peaks	Interplanar distance obtained by synchrotron XRD (in Å)	Interplanar distance obtained by HR-TEM (in Å)
101	3.93	3.93
121	2.78	2.78
220	2.27	2.27
202	1.96	1.96
123	1.60	1.60
242	1.38	1.38
204	1.24	1.24

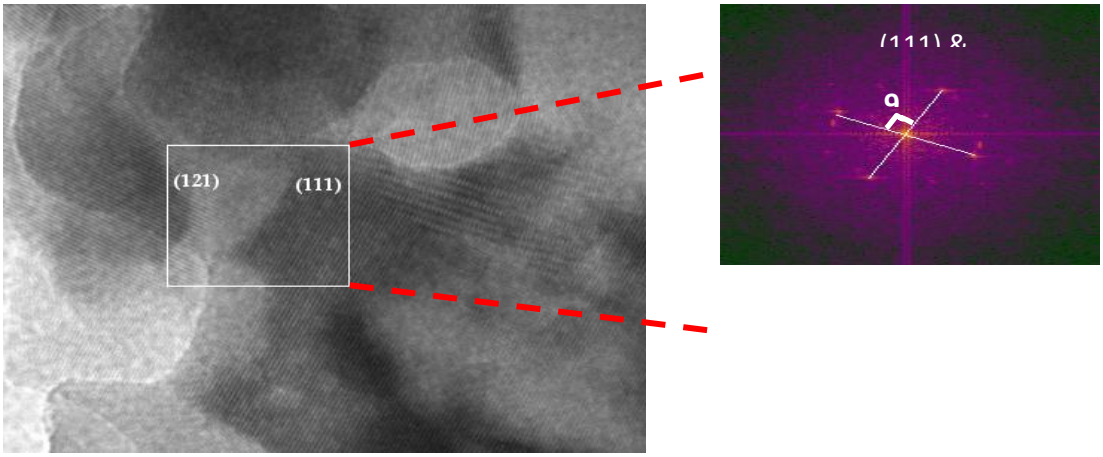

Figure 17.The FFT patterns for HR-TEM of the perovskite $La_{0.7}Y_{0.3}FeO_3$, corresponding to (121) and (111) plane.

4. Conclusion

Multiferroic $La_{1-x}Y_xFeO_3$, (X=0.0, 0.05, 0.1, 0.15, 0.25 and 0.3) perovskites have been successfully synthesized through Sol-gel auto-combustion method. A structural analysis by room temperature synchrotron X-ray diffraction (XRD) analysis confirms the single phase character of all the compositions with orthorhombic structure having space group Pnma (No.62), without any impurity phase. The tolerance factor confirmed the phase stability of the prepared compositions. The values of the tolerance factor decreased with increasing Y content at the expense of La^{3+} due to the difference in the ionic radii of both La^{3+} and Y^{3+} ions. The Williamson-Hall plot based on synchrotron XRD data was used to estimate the average particle diameter of different perovskite compositions and show variety from 18 nm to 27.8 nm.

The structure of the perovskite $La_{1-x}Y_xFeO_3$, (X=0, 0.05, 0.1, 0.15, 0.25 and 0.3) nanocrystallites were further analyzed by HRTEM micrographs, and indicated that the particles of the perovskite samples are semi-spherical in shape and is quite close to the X-ray crystallite size. However, some particles are quite bigger due to the agglomeration of small grains and variation of density of it clearly corroborates the findings. The SAED patterns of the prepared orthoferrites showed spotty ring patterns signifying a formation of polycrystalline orthorhombic structure with (SG: Pnma), without any spot related to any impure phases, and consistent with XRD results. The electron density map and MEM, show the increase in density around lanthanum cation (A-site),and relatively large displacements in the various oxygen positions in the unit cell as compared to the Fe, Y and La positions, where strong positive peaks corresponding to the 4c sites.

The M(H) hysteresis loops of the prepared $La_{1-x}Y_xFeO_3$ multiferroic system were measured at room temperature by VSM in the field varies between +20 kOe to -20 kOe and exhibited soft ferromagnetic behavior, this behavior showed that the ferromagnetism is owing to the uncompensated spins at the surface and the canted spin, which is the nature of size-induced magnetism on nanoparticles. The M(T) and M(H) curves of the prepared perovskites show weak ferromagnetic behavior. The M(H) curve for pure $LaFeO_3$ perovskite confirms weak ferromagnetic character with the maximum magnetization (M) at 20 kOe of ~1.76 emu/g and H_C of ~125 Oe. The positive paramagnetic Weiss temperature indicating the ferromagnetic behavior of the prepared $LaFeO_3$ perovskite.

Acknowledgment

The authors acknowledge the support provided by IUPAP-IUCr LAAMP within the ICSU Grants Programme 2016-2019. We would like to express special thanks for experimental assistance to Jasper Rikkert (MCX

beamline scientist- Elettra synchrotron- Trieste- Italy) and Lara Gigli (postdoc in MCX beamline- Elettra synchrotron- Trieste- Italy).

References

[1] N.A.Spaldin, Topics Appl. Physics, vol.105, pp.175–218, (2007).

[2] D.I.Khomskii, J. Magn. Magn. Mater. vol.306, Issue 1, pp.1–8, (2006).

[3] J.F.Scott, Nature Mater, vol. 6,Issue 4, pp. 256–257,(2007).

[4] N.A. Spaldin, S.W. Cheong, R. Ramesh, Phys. Today, vol. 63, Issue 10, pp.38-43,(2010).

[5] N.A. Hill, J. Phys. Chem. B, vol.104, Issue 29,PP. 6694–6709,(2000).

[6] N.A. Hill, Annu. Rev. Mater. Res., vol.32, Issue 1, pp.1–37,(2002).

[7] M. Idrees, M. Nadeem, M. Atifc, M. Siddique, M. Mehmood, M.M. Hassan, Acta Mater, vol. 59, Issue 4, pp.1338–1345,(2011).

[8] W. Zheng, R. Liu, D. Peng, G. Meng, Mater. Lett., vol. 43,Issue 1-2, pp. 19–22 (2000).

[9] C. Shivakumara. Solid State Comm., vol. 139,pp. 165-169,(2006).

[10] A.D. Jadhav, A.B. Gaikwad, V. Samuel, V. Ravi, Mater. Lett.,Vol. 61, Issue 10,pp. 2030–2032 (2007).

[11] A.A. Cristobal, P.M. Botta, P.G. Bercoff, E.F. Aglietti, H.R. Bertorello, J.M. Porto Lopez, J. Alloys Compd.,Vol. 495, Issue 4,pp. 516–519 (2010).

[12] N.W. Grimes, R.J. Hilleard, J. Waters, J. Yerkess, J. Phys. C (Prog. Phys. Soc.), vol. 1, Issue 3,pp. 663–672, (1968).

[13] G. Blasse, Philips Res. Repts Suppl.,vol. 3, Issue 3, p. 91, (1964).

[14] G.E. Bacon, F.F. Roberts, ActaCrystallogr.,vol. 6,pp. 57–62, (1953).

[15] M. Marezio, P.D. Dernier, Mater. Res. Bull. vol. 6, pp.23–30,(1971).

[16] H. M. Rietveld, ActaCrystallogr., vol. 22, Issue 1, pp.151–152, (1967).

[17] H. M. Rietveld, J. Appl. Crystallogr. vol. 2, Issue 2, pp.65–71, (1969).

[18] R. J. HILL, J. Appl. Crystallogr., vol. 25, Issue 5, pp.589–610, (1992).

[19] S. Bid, S.K. Pradhan, J. Appl. Crystallogr. vol.35, Issue 5, pp.517-525, (2002).

[20] S. Bid, S. K. Pradhan, Mater. Chem. Phys. vol. 82, Issue 1, pp. 27-37, (2003).

[21] H. Dutta, S.K. Manik, S.K. Pradhan, J. Appl. Crystallogr. vol. 36, Issue 2, pp.260–268, (2003).

[22] S. K. Manik, S. K. Pradhan, Mater. Chem. Phys., vol. 86, Issue 2, pp. 284-292, (2004).

[23] Y. M. Abbas, A. Bakry M., A. Hassan Ibrahim, American J. Mat. Sci.,vol.4, Issue 2, pp. 84-96(2014).

[24] A.A. Cristóbal, P.M. Botta, E.F. Aglietti, M.S. Conconi, P.G. Bercoff, J.M. Porto

López, Mat. Chem. Phys.,vol. 130, Issue 3, pp.1275–1279,(2011).

[25] M. Birkholz, Thin Film Analysis by X-ray Scattering. Wiley-VCH Verlag GmbH and Co. KGaA, Weinheim, (2006).

[26] H. Kronmller, Stuart, M. Johnsson, P. Lemmens (2007). Handbook of magnetism and advanced magnetic materials. Hoboken, NJ: John Wiley & Sons, (2012).

[27] R.L. Cook, A.F. Sammells, Solid State Ion.,vol. 45, Issue 3–4, pp.311–321, (1991).

[28] S. Komine and E. Iguchi, J. Phys. Chem. Solids, vol. 68, Issue 8, pp. 1504–1507, (2007).

[29] A. V. Galubkov, E. V. Goncharova, V. P. Zhuze, and I. G. Manilove, Sov. Phys. Sol. State, vol. 7, Issue 8, pp. 1963–1967, (1966).

[30] E. A. Jaiswal, R. Das, K. Vivekanand, P. M.Abraham, S. Adyanthaya, P. Poddar, J. Phys. Chem. C, vol. 114, Issue 5, pp. 2108–2115, (2010).

[31] W. J. Schuele, V. D. Deetscreek, J. Appl. Phys., vol. 33, Issue 3, pp. 1136–1137, (1962).

[32] Y. Shimakawa, M. Azuma, and N. Ichikawa, J. Materials, vol. 4, Issue 1, PP. 153–168, (2011).

[33] F.C. Fonseca, A. S. Ferlauto, F. Alvarez, G. F. Goya, and R. F. Jardim, J. Appl. Phys., vol. 97, Issue 4, pp. 04431371-04431372, (2005).

[34] A. Sommerfeld and H. Beterm, H. Geiger , K. Scheel (Eds) Handbuch der Physik, Berlin: Springer, vol. 24, Issue 2, p. 595, (1933).

[35] E. Lima Jr., T.B. Martins, H.R. Rechenberg, G.F. Goya, C. Cavelius, R. Rapalaviciute, S. Hao and S. Mathur, J. Mag. Magn. Mat., vol. 320, pp.622–629,(2008).